JOURNAL OF MATERIALS SCIENCE 11 (1976) 892–902

The relationship between ductility and grain-boundary precipitates in an Al-6.0% Zn-2.6% Mg alloy

TAKESHI KAWABATA, OSAMU IZUMI
The Research Institute for Iron, Steel and Other Metals, Tohoku University, Sendai, Japan

The relationship between ductility and material parameters such as grain-boundary (GB) precipitate size and dimple size in an Al–6.0% Zn–2.6% Mg alloy has been studied. Under the condition of a given GB precipitate size, the ductility increases with decreasing number of GB precipitates and dimples per unit area. The critical GB precipitate sizes acting as the nuclei for void formation are deduced.

1. Introduction

Al–Zn–Mg alloys are known for their high strength among the aluminium-base alloys, but they exhibit a serious defect which is the occurrence of intergranular fracture. Geisler [1] was the first to suggest that the brittleness is due to preferential deformation within precipitate-free zones (PFZ) adjacent to grain boundaries (GB) whilst Ryder and Smale [2] showed that GB precipitates act as the nuclei for void formation. According to Unwin and Smith [3], the fracture toughness decreases with the area fraction of GB precipitates and is independent of the PFZ width. However, Ryum [4] has proposed an idea that the PFZ contributes to the increase of ductility. There are many problems which must be clarified concerning the relationship between the ductility and PFZ and the role of GB precipitates in intergranular fracture. No quantitative discussion has previously been made about the critical size of GB precipitates acting as the effective nucleation sites for void formation.

The purpose of the present investigation is, therefore, to make clear the following:

(1) the relationship between ductility and material parameters, especially the size and the distribution of GB precipitates;

(2) the relationship between ductility and characteristics of the fracture surface such as the size of dimples;

(3) the critical size of GB precipitates for void formation.

2. Experimental procedures

An Al–6.0% Zn–2.6% Mg alloy was prepared using 99.99 wt % purity aluminium, 99.99% purity zinc and a magnesium master alloy (Mg: 11.00%, Si: 0.056%, Fe: 0.255%, Cu: 0.02%, Al: balance). After degassing by bubbling N_2 gas for 10 min at 750° C, the melt was held static for 15 min, then cast in a metal mould 110 mm x 110 mm x 270 mm held at 150° C. The surface of the ingot was machined to a depth of ~7 mm, and then homogenized for 24 h at 460° C, following which it was

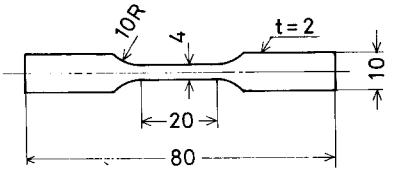

Figure 1 The shape and dimensions of a tensile specimen (mm).

hot-forged and hot- and cold-rolled to 2 mm thick sheet. The shape of the tensile specimen machined from the plate is shown in Fig. 1. It has a gauge length of 20 mm, width of 4 mm and 2 mm thickness. For structural observations with the transmission electron microscope, 0.2 mm thick plates

TABLE I The chemical compositions of specimen (wt %).

	Zn	Mg	Fe	Si
Al–Zn–Mg	6.0	2.6	< 0.001	0.012

were prepared by cold-rolling the 2 mm thick plates. The result of the chemical analysis is shown in Table I.

The specimens were solution-treated for 1 h at 460° C and quenched into water at room temperature. Then they were aged in oil-baths held at fixed temperatures. Two-stage ageing treatments were used, the initial stage being carried out at 100° C for y sec ($y = 0$, 30, 300, 3000, 30 000, and 300 000 sec), and the final stage at 160° C for z h (1 to 4 h). The second stage ageing times were selected so that specimens were aged to peak hardness. Fig. 2 shows a schematic diagram of the applied heat-treatment schedule. Tensile tests were

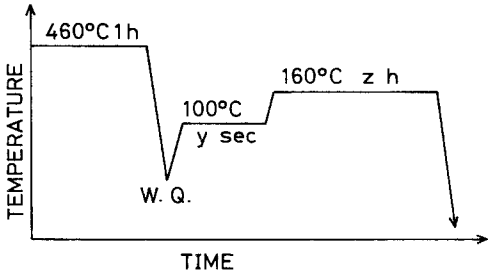

Figure 2 The applied heat-treatment.

performed at room temperature using an Instron-type testing machine with an initial strain-rate of 0.025 min^{-1}. Micro-Vickers hardness measurements were also performed with a 500 g load. The structure was observed by optical and transmission electron microscopy (JEM-6) carried out at 100 kV. Fracture surfaces were observed by the two-step carbon replica technique employing a JEM-SS (Super-Scope).

3. Experimental results and discussion

3.1. Results of structural observations with the optical microscope

Fig. 3a, b and c are optical micrographs showing a rolled surface, a longitudinal section and a transverse section respectively, in a specimen of 2 mm thick plate. All show equi-axed crystals and the grain sizes are approximately equal.

3.2. Results of structural observations with the transmission electron microscope

3.2.1. GB precipitates

Fig. 4a, b and c are examples of transmission electron micrographs. As seen in these micrographs, GB precipitates and PFZs are formed along the GBs

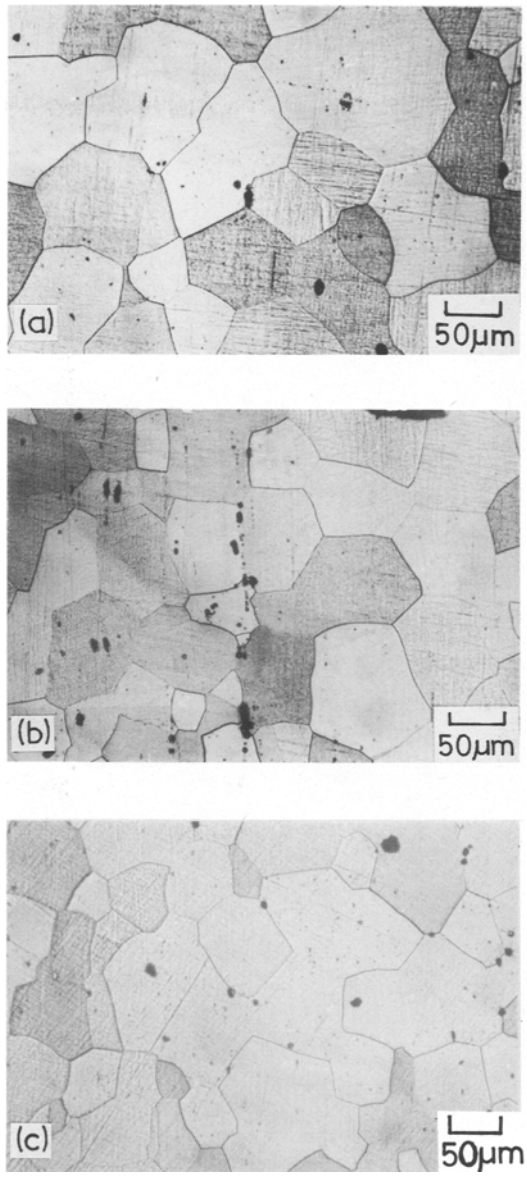

Figure 3 Optical micrographs of the structure in an Al–6.0% Zn–2.6% Mg alloy. (a) The rolled surface, (b) longitudinal section, (c) transverse section.

in the aged condition. The size and distribution of the GB precipitates were measured on the micrographs of about 20 plates similar to that shown in Fig. 4b. The shape of a GB precipitate can be regarded as an ellipse and the long and short axes are measured individually. Based on these measurements, frequency distribution diagrams are drawn up. These are illustrated in Fig. 5a to e. The positions of the peaks in the frequency distribution diagrams tends to shift slightly to the smaller size of particles with increasing pre-ageing time.

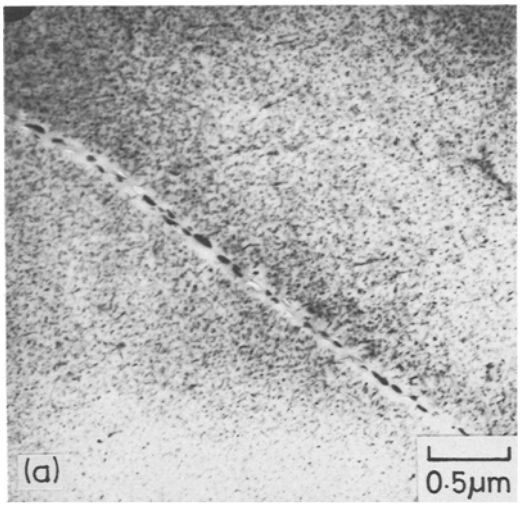

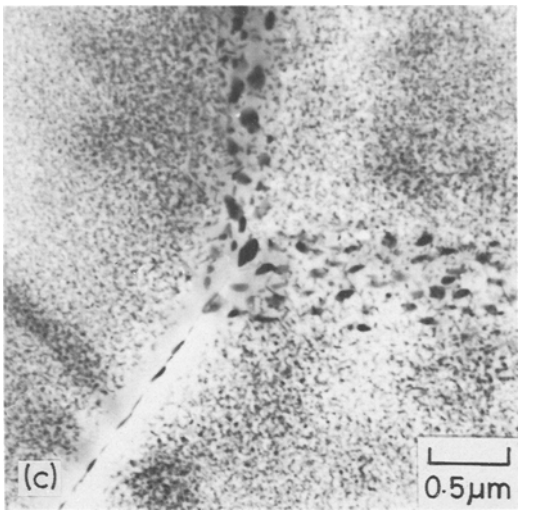

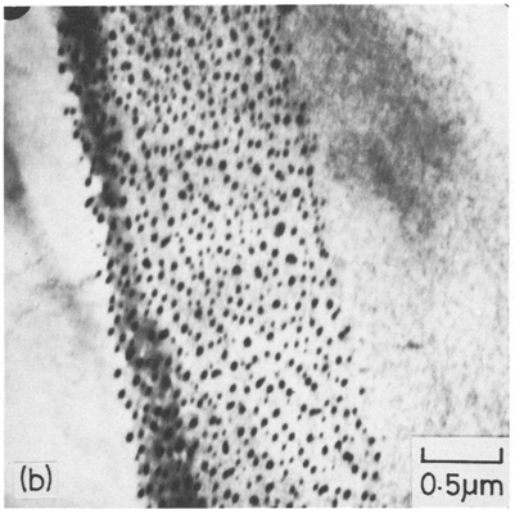

Figure 4 Examples of the transmission electron micrographs of the aged structure in an Al–6.0% Zn–2.6% Mg alloy. (a) The microscructure near the GB in the parallel direction to the GB; (b) typical micrograph from which the size and distribution of GB precipitates are measured. The GB lies at a small angle to the paper; (c) micrograph showing the triple point which is constructed from GBs inclined at different angles to the paper.

It is interesting that the shape of the frequency distribution diagrams in the present study is different from those proposed theoretically [5, 6]. The theoretically determined particle size distribution is shown in Fig. 14. Quite recently, Koiwa [7] has developed the kinematical theory of precipitation process in solid solutions. His calculation shows that if the back reaction is neglected and if the size-dependent reaction is assumed, the frequency distribution curve of the particle size decreases gradually with increasing particle size in the region beyond the peak. This feature of a gradual cut off is different from the steep ones of Lifshitz and Slyozov [8], Asimow [9], Ardell [6] and Kirchner [5].

Based on the frequency distribution diagrams, the average sizes of GB precipitates are calculated for the single- and two-step aged specimens. The result is illustrated in Fig. 6. Irrespective of the large variance of the pre-ageing time at 100° C, the average sizes of GB precipitates are approximately constant, although somewhat lower values are seen at 3×10^4 and 3×10^5 sec. This suggests that the average size of GB precipitates should not be determined by the pre-ageing time at 100° C, but by the subsequent ageing time at 160° C, i.e. if the subsequent ageing times are approximately equal, the sizes of the resulting GB precipitates will be similar. In this series of experiments, second-stage ageing times were not the same, as they were selected to give peak hardness for the final condition.

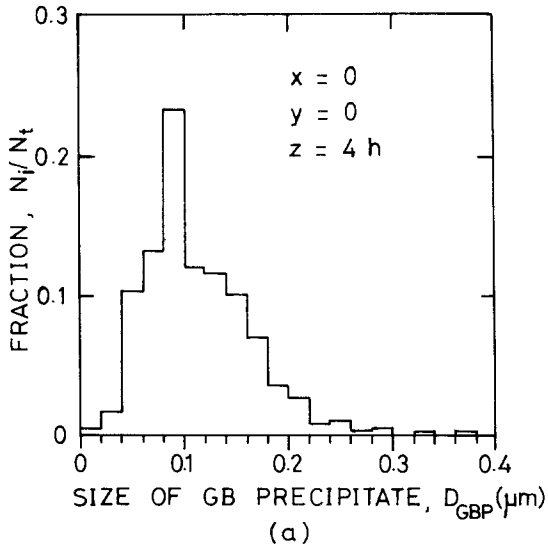

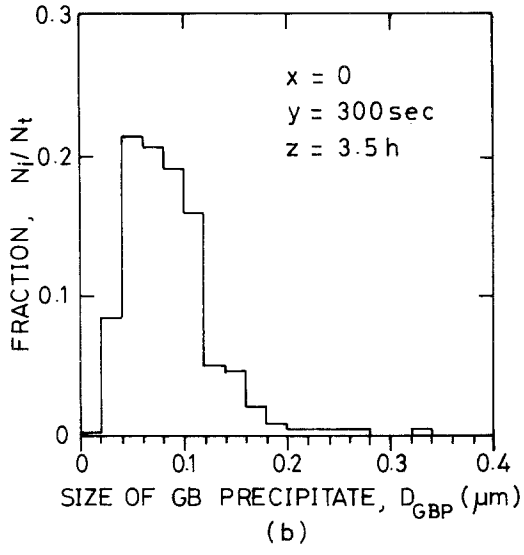

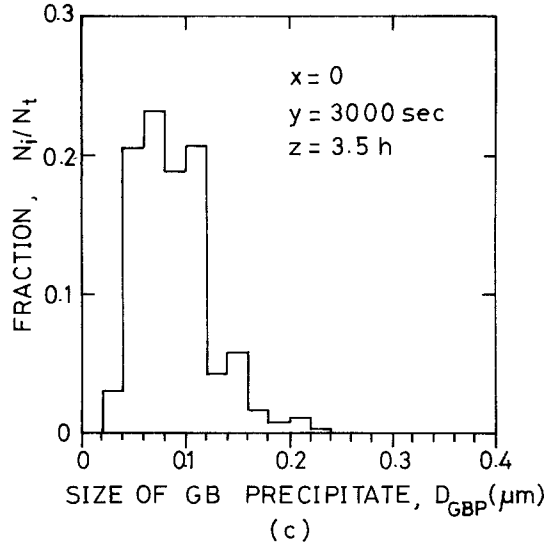

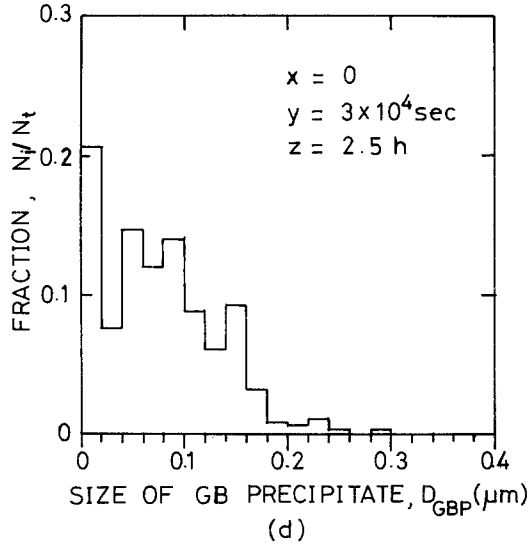

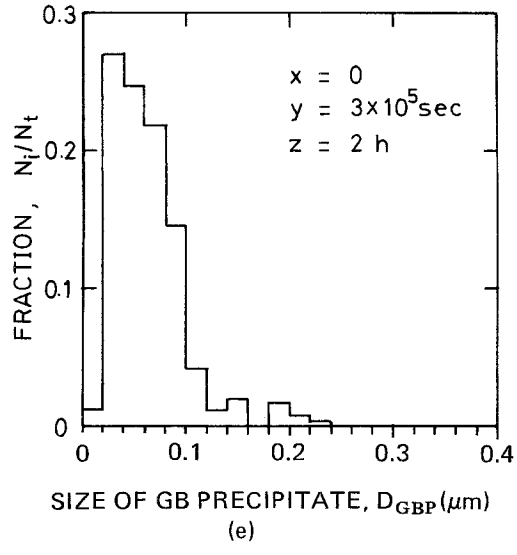

Figure 5 The histogram of the frequency distribution for the sizes of GB precipitates in an Al–6.0% Zn–2.6% Mg alloy. Ageing treatments are (a) $y = 0$, $z = 4$ h, (b) $y = 300$ sec. $z = 3.5$ h, (c) $y = 3000$ sec, $z = 3.5$ h, (d) $y = 3 \times 10^4$ sec, $z = 2$ h, (e) $y = 3 \times 10^5$ sec, $z = 2$ h.

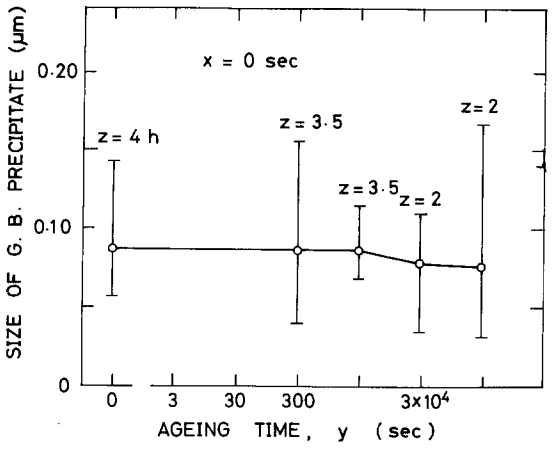

Figure 6 The effect of the pre-ageing time at 100° C on the average sizes of GB precipitates.

3.2.2. The width of PFZ

Widths of PFZ (w) against various pre-ageing times are tabulated in Table II. The width decreases with pre-ageing time. However, no meaningful correlation between the width and the ductility could be recognized.

There is experimental evidence to support each of the three possible effects of PFZ on mechanical properties, and in particular ductility, i.e. that the PFZ is (1) harmful to ductility [1, 10, 11], (2) increases the ductility [4] and (3) has no effect on the ductility [3, 12–14]. The experimental results, concerning the third idea, have been detailed by Abe *et al.* [14]. According to them, the width of PFZ has no influence upon the uniform elongation but does influence the non-uniform elongation (i.e. the elongation from the beginning of necking to the fracture decreases with the width of PFZ). However, their conclusion seems to be drawn without any attention to the size of GB precipitates and the decrease in the elongation which, they observed, might be due to the increase of the size of GB precipitates.

3.3. Results of mechanical tests

The results of the mechanical tests are shown in Table II. Stress levels of $\sigma_{0.2}$ and σ_{UTS} in the range of $y \geqslant 300$ sec are larger by about 20% than those for $y \leqslant 30$ sec, indicating the effect of two-step ageing. Nominal strains to fracture, ϵ_f, nominal strains to ultimate stress, ϵ_{UTS}, and true fracture strains, ϵ_f^{true} $[= \ln (A_0/A)]$, are also tabulated. These strains decrease with pre-ageing time except for $y = 3 \times 10^4$ sec.

3.4. Results of fracture surface observation

3.4.1. The observation of GB fracture

Aged specimens had strains to fracture ranging from a few percent to over 10%, and fracture occurred after necking. Scanning electron micrographs were taken of the fractured specimen surfaces close to, and away from, the fractur surface as shown in Fig. 7a and b, respectively. The crystalline grains in the fracture part are considerably elongated along the tensile direction but the fracture, however, occurs intergranularly. At some distance from the fracture part, GB cracks are also observed (Fig. 7b).

3.4.2. The fracture surfaces and the heat-treatment conditions

Fig. 8a and b are electron micrographs of the fracture surfaces of single- and double-aged specimens, respectively. Typical ductile fracture surfaces formed from equi-axed dimples are observed in both micrographs. It is apparent that there are some differences in the microstructures of the fracture surfaces. That is, the fracture surface of specimens treated by single-step ageing, compared to that of the two-step ageing, is remarkably rougher and contains larger dimples. In a few dimples in Fig. 8a the traces of precipitate which may contribute to the dimple formation by acting as nuclei can be observed.

TABLE II Heat-treatment (y, z), results of mechanical tests ($\sigma_{0.2}$, σ_{UTS}, ϵ_{UTS}, ϵ_f, ϵ_f^{true}), results of the observations of fracture surfaces ($\bar{D}_D$) and the microstructure (w, D_{GBP}), and the deduced critical sizes of GB precipitates (D_{GBP}^{crit}).

y (sec)	z (h)	$\sigma_{0.2}$ (kg mm^{-2})	σ_{UTS} (kg mm^{-2})	ϵ_{UTS}	ϵ_f	ϵ_f^{true} $\ln \frac{A_0}{A}$	w (μm)	$\bar{D}_D$ (μm)	D_{GBP} (μm)	D_{GBP}^{crit} (μm)
0	4	26.3	35.2	0.109	0.149	0.53	0.126	1.44	0.116	0.24
300	3.5	29.9	48.3	0.103	0.133	0.26	0.096	0.64	0.087	0.16
3000	3.5	42.0	48.5	0.051	0.079	0.34	0.073	–	0.088	–
3×10^4	2	40.7	49.3	0.104	0.130	0.32	0.048	0.72	0.078	0.16
3×10^5	2.5	45.2	50.0	0.063	0.069	0.16	0.042	0.60	0.076	0.16

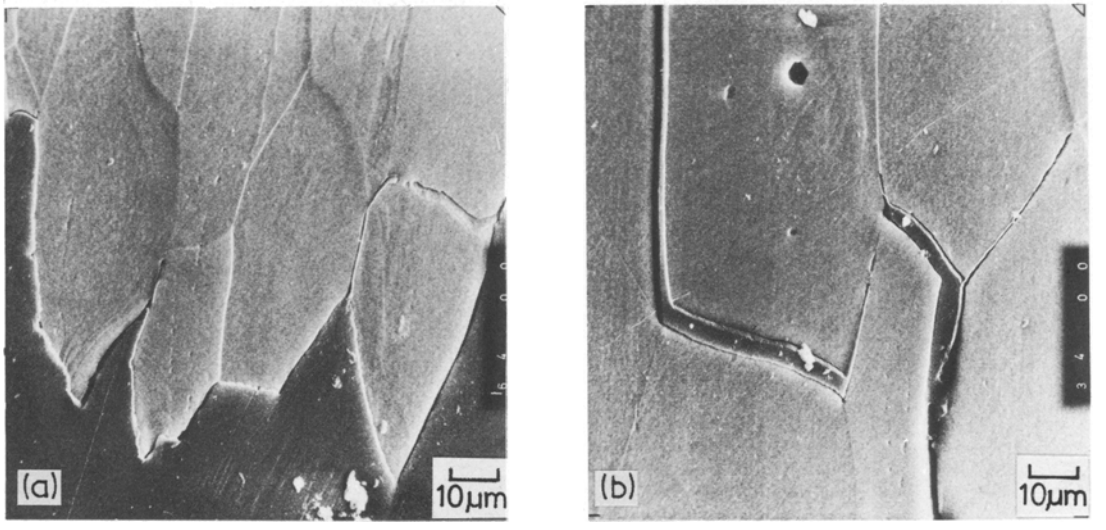

Figure 7 Appearances of the GB fracture (a) at the fracture portion and (b) in the same region at a short distance from the fracture portion. The specimen was solution-treated at 460° C for 1 h, water-quenched to room temperature, pre-aged at 100° C for 3000 sec, and subsequently aged at 160° C for 3.5 h.

3.4.3. The frequency distribution of dimple sizes

Fig. 9a to d illustrate the frequency distribution diagrams of dimple sizes in specimens given two-step ageing treatments. The class interval is 0.2 μm. The maximum number of dimples occurs in the range 0.6 to 0.8 μm diameter. Beyond this range, the frequency decreases gradually with increasing size. Very large dimples about 6 to 7 μm were also observed. The shapes of these curves are similar to those of the frequency distributions of GB precipitates. The average size of dimple ($\bar{D}_D$) corresponding to various pre-ageing times (y) is tabulated in Table II. The values of $\bar{D}_D$ change corresponding to the values of ϵ_f.

3.5. Relationships between the fracture strain and the dimple size, and the density of GB precipitates

If the density of voids formed by the plastic deformation is large, then the voids will begin to coalesce whilst still at a small size, but if the initial

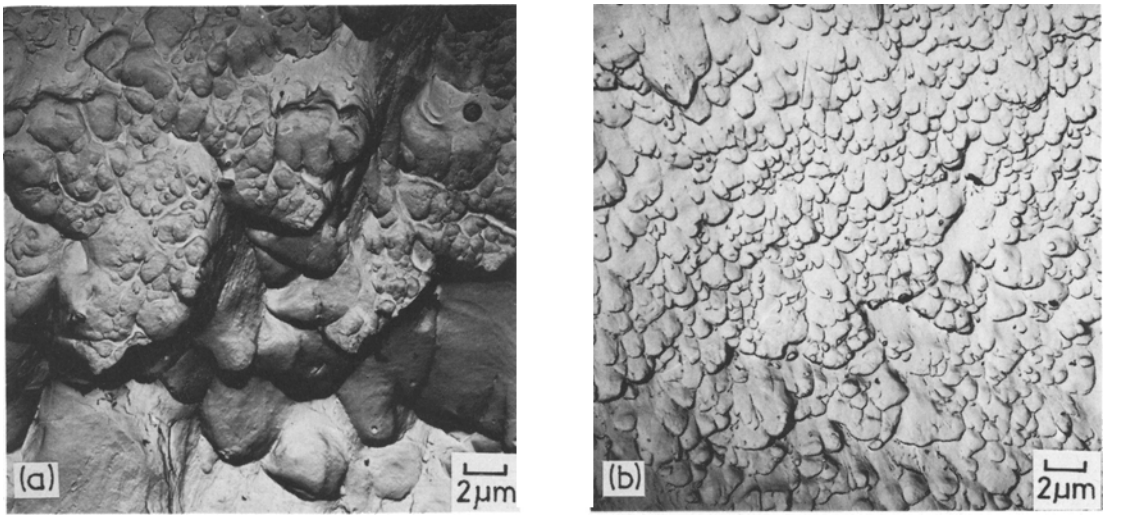

Figure 8 Electron micrographs of a replica showing the variation of appearances of the fracture surface due to heat-treatment. Specimens are solution-treated at 460° C for 1 h, water-quenched to room temperature: (a) aged at 160° C for 4 h; (b) pre-aged at 100° C for 3000 sec, and subsequently aged at 160° C for 3.5 h.

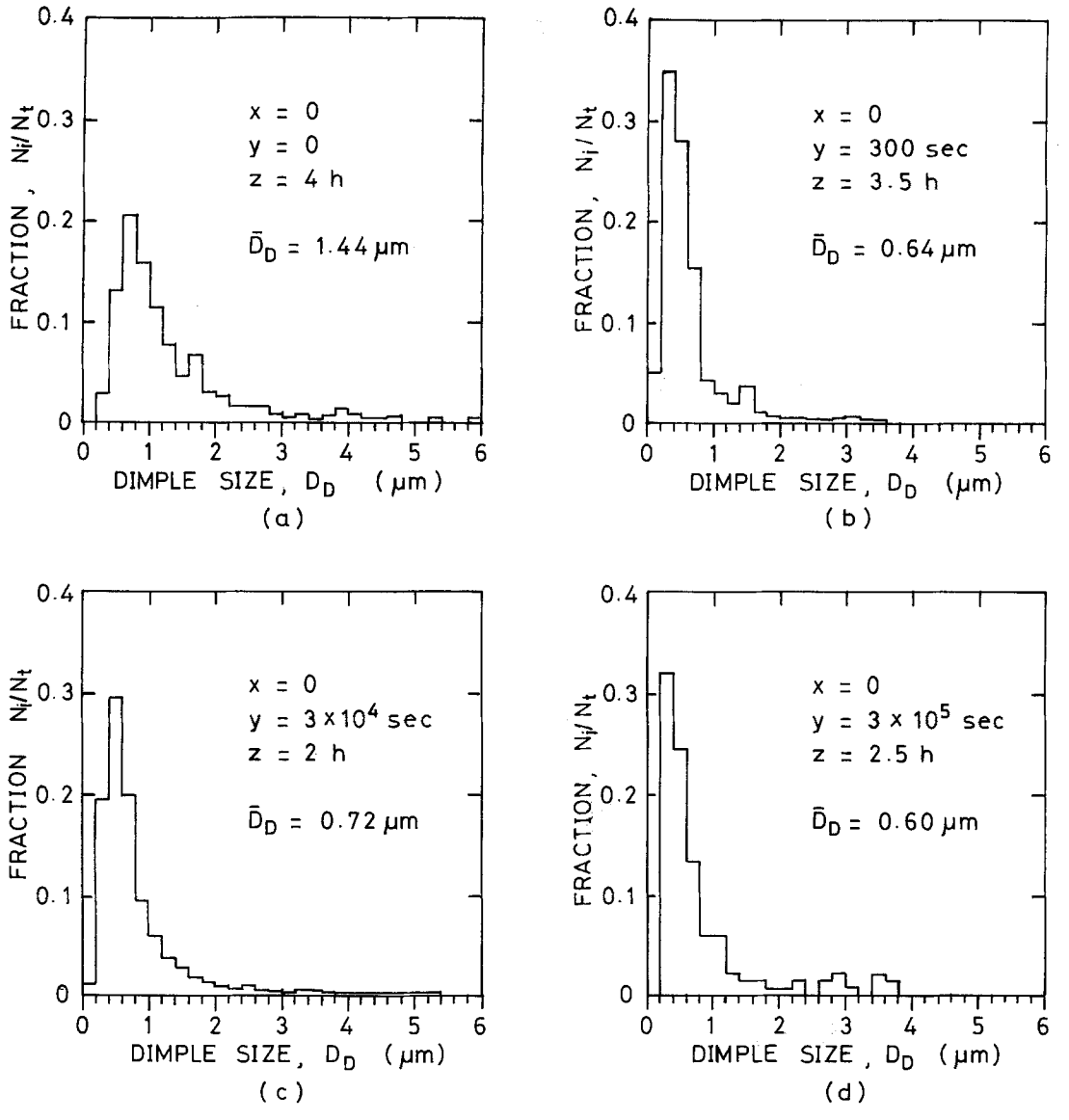

Figure 9 Histograms of the frequency distribution of dimple sizes in specimens aged (a) $y = 0$, $z = 4$ h, (b) $y = 300$ sec, $z = 2$ h, (c) $y = 3 \times 10^4$ sec, $z = 2$ h, (d) $y = 3 \times 10^5$ sec, $z = 2.5$ h.

density is small, then the voids will grow before coalescence. The dimple size is equal to the void size at coalescence and the strain which is required for the void growth increases with the final size of voids so that the dimple size is closely related with the ductility. Furthermore, if it can be assumed that the GB precipitates act as the nuclei for the formation of microvoids, and one microvoid grows to one large void, the density of the GB precipitates acting as nuclei is related to the ductility. That is, the smaller the density of nuclei, the larger the dimple size and, consequently, the larger the strain to fracture. The above ideas are shown schematically in Fig. 10. In order to verify the above consideration, the relationships between the strain to fracture and the dimple size, and the density of GB precipitates were investigated experimentally.

Fig. 11 shows the fracture strain in relation to the number of dimples per unit GB area. The smaller the number of dimples, the larger is the fracture strain.

The density of GB precipitates was plotted against the fracture strain as shown in Fig. 12. The average sizes of these GB precipitates were approximately equal (Fig. 6), so that the relationship between the densities of GB precipitates and the

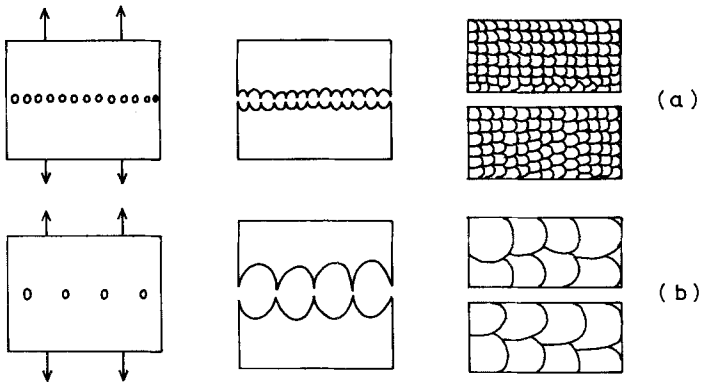

Figure 10 Schematic diagram showing the relationship between the density of voids and the fracture strain. Cases in which the density of voids is (a) large, and (b) small.

fracture strain corresponds to that between the volume fraction of GB precipitates and the fracture strain, i.e. the curve in Fig. 12 corresponds approximately to that obtained by Edelson *et al.* [15]. It seems that the experimental results support the discussion in the initial part of this section, i.e. the dimple size and the density of GB precipitates are closely related to the fracture strain.

3.6. Estimation of the GB precipitate size which can act as the nucleus of a void

Dimples formed on the fracture surface are considered to be halves of voids at coalescence [16]. The relationships between the dimple size, the density of GB precipitates and the ductility have already been discussed in the previous section. If we can deduce the condition under which GB precipitates act as nuclei for void formation, we will be able to estimate the critical size for nucleation.

The following sources for void nucleation within the PFZ can be considered:

(1) decohesion at the interface between the GB precipitates and the matrix [2];

(2) the fracture of the GB precipitate itself;

(3) the interaction between dislocations in the PFZ.

With regard to source 1 in the present investigation, precipitates were rarely observed in dimples and those that were observed were relatively large precipitates (Fig. 8a and b).

Goto and Koda [22] have shown by investigating the transgranular fracture surfaces of three aluminium alloys (1100, 3003 and Al–4% Cu alloy) that the one-to-one relationship between dimples and particles is realized. According to them, when no precipitates were initially observed in dimples they could be subsequently revealed in all of them by lightly etching the fracture surfaces. Therefore, in the present investigation, it is considered that the precipitates cannot be observed because they lie just under the surfaces of the dimples.

With regard to source 2, the fracture of particles has been observed at large particle sizes [17–22].

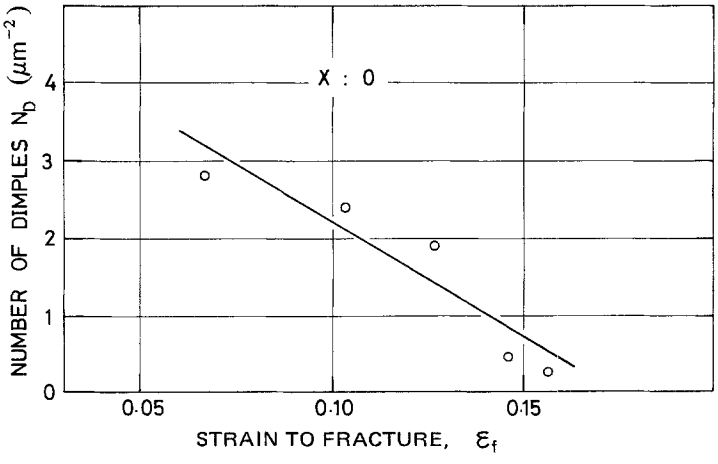

Figure 11 The relationship between the number of dimples per unit area and the strain to fracture.

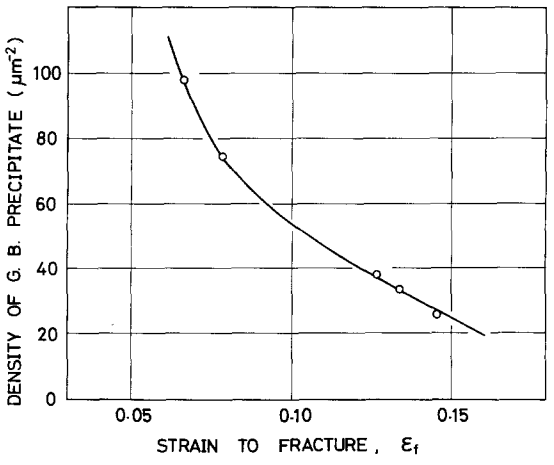

Figure 12 The relationship between the density of GB precipitates and the strain to fracture.

With regard to source 3, the following may be considered: (a) the interaction between the additional dislocations occuring around the GB precipitates according to Ashby's theory [23]; (b) the interaction between dislocations disregarding the existence of the GB precipitates.

Bauer and Wilsdorf [24] have reported a case where, in the fracture of a stainless steel, not all voids in the ductile fracture were initiated at particles, the ratio of the average void density to the average particle density being of the order of 100. Therefore, they proposed a mechanism by which an interaction between dislocations and vacancies nucleates voids. However, no evidence of such interactions has been found [24].

In (1), (2) and (3a), the GB precipitates are concerned in void formation. As described in the introduction, the larger the particle size, the easier is void nucleation [25]. Therefore, we conclude that the statistical distribution of the size of GB precipitates is important (strictly speaking, (i) the size (ii) the morphology and (iii) characteristics such as the chemical composition or structure, of precipitates should be taken into account for the formation of voids).

Once a void has been formed, it would grow and relieve the strain around it. Then, on the interfaces of other precipitates existing in a given region around the void, further nucleation of voids might be difficult because of the strain relief effect due to the void initially formed. Therefore, only some of the GB precipitates would contribute to void formation.

Fig. 13 illustrates the relationship between N_D (the number of dimples per unit area) and N_{GBP} (the density of GB precipitates) in specimens given the same heat-treatment. In the figure the ratio, N_{GBP}/N_D, is also shown. This means that dimples are formed in the ratio of 1 : 20 to 1 : 40 GB precipitates.

The size of GB precipitate which acts as a nucleus can be deduced as follows. Initially, two assumptions are made, i.e. (1) if the strain is equal around precipitates, the larger the size of precipitate, the easier is void formation, (2) one void grows, coalesces with other voids and then forms one dimple.

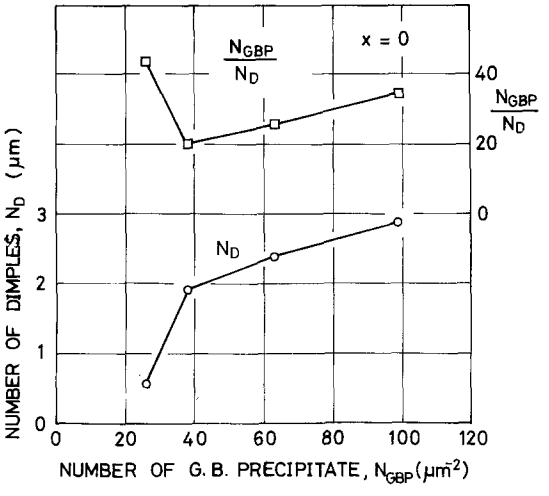

Figure 13 The relationship between the number of dimples per unit area, N_D and the number of GB precipitates, N_{GBP}, and the ratio, N_{GBP}/N_D, when specimens are solution-treated at 460° C for 1 h, water-quenched to room temperature, pre-aged at 100° C for various periods and subsequently aged at 160° C for the period required to reach maximum hardness.

For simplification, the frequency distribution diagram of GB precipitate sizes is replaced by the density distribution function $n(D)$. This is shown schematically in Fig. 14a. $n(D)$ is normalized so that

$$\int_0^\infty n(D)\,dD = 1, \tag{1}$$

where D is the size of GB precipitate. Integrating $n(D)$ from zero to D the distribution function $F(D)$ is obtained. This is shown in Fig. 14b.

$$F(D) = \int_0^D n(D)\,dD. \tag{2}$$

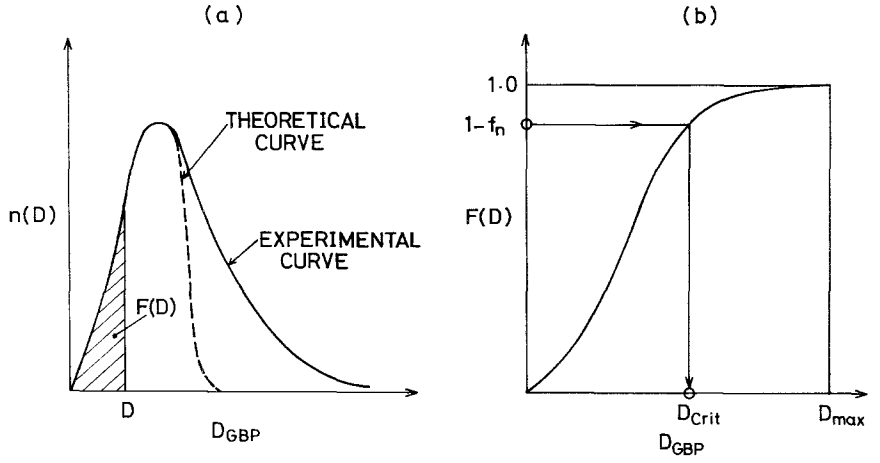

Figure 14 The frequency distribution function ($n(D)$), the cumulative frequency distribution function ($F(D)$) of GB precipitates and the method used to deduce the critical size of GB precipitates.

The critical size of the GB precipitate for void formation, D_{crit}, is deduced from Fig. 14b by putting

$$F(D) = 1 - f_n, \tag{3}$$

where f_n is the ratio of the number of dimples to GB precipitates per unit area.

The corresponding equations obtainable from the histograms are:

$$\sum \frac{N_i}{N_t} = \sum_i f_i = 1 \tag{4}$$

$$F(D_i) = \sum_{j=1}^{i} f_j \tag{5}$$

$$F(D_i) = 1 - f_n \tag{6}$$

where N_i is the number of GB precipitates in the class i, N_t is the total number of GB precipitates, f_i the fraction of GB precipitates in the class i, D_i the nominal diameter of GB precipitates in the class i, D_i obtained from Equation 6 gives the critical size of precipitate for void nucleation. The critical size of precipitate (D_{crit}) obtained for various heat-treatments is shown in Table II.

Whenever the pre-ageing time at 100° C exceeds more than 300 sec or two-step ageing is used, the values of D_{crit} are 0.16 μm. However, for single-step ageing, D_{crit} is 0.24 μm.

The difference in D_{crit} caused by the different ageing treatments might be related to the variation of precipitation within the grains, i.e. to the variation of the critical shear stress within the grains. That would be considered as follows.

The dislocation density will be lower in the PFZ when dislocations can move more easily from the PFZ to the interior of grains. The strain which is required to give fracture at the interfaces between GB precipitates and matrix will increase with the decrease in the size of GB precipitates. Therefore, if there is a critical value in the dislocation density within the PFZ corresponding to the difference between the critical resolved shear stress within PFZs and that in the interior of grains, there will be a threshold value in the critical precipitate size for void nucleation because of the limit of the dislocation density.

4. Conclusions

Tensile tests, observations of the fracture surfaces and microstructures have been carried out on an Al-6.0% Zn-2.6% Mg alloy and the following results are obtained.

(1) The strains to fracture increase with increasing dimple size and with decreasing number of GB precipitates per unit area.

(2) The number of GB precipitates per unit area does not coincide with the number of dimples and it is considered that only one in 20 to 40 of the GB precipitates acts as a void nucleus.

(3) The values of D_{crit} obtained were 0.24 and 0.16 μm in the specimens given single and two-step ageing treatments, respectively.

Acknowledgements

The authors are grateful to Emeritus Professor S. Shimodaira and Mr T. Sato for the use of the

scanning electron microscope. The authors also wish to thank the Keikinzoku Shogakukai (The Light Metal Educational Foundation, Incorporated) for their support.

References

1. A. H. GEISLER, "Phase Transformations in Solids", edited by R. Smoluchowski *et al.* (Wiley, New York, 1951) p.387.
2. D. A. RYDER and A. C. SMALE, "Fracture of Solids" edited by D. C. Drucker and J. J. Gilman (Interscience, New York, 1963) p.237.
3. P. N. T. UNWIN and G. C. SMITH, *J. Inst. Metals* **97** (1969) 299.
4. N. RYUM, *Acta Met.* **16** (1968) 327.
5. H. O. K. KIRCHNER, *Met. Trans.* **2** (1971) 2861.
6. A. J. ARDELL, *Acta Met.* **20** (1972) 61, 601.
7. M. KOIWA, *Phil. Mag.* **30** (1974) 877.
8. I. M. LIFSHITZ and V. V. SLYOZOV, *J. Phys. Chem. Solids* **19** (1961) 35.
9. R. ASIMOW, *Acta Met.* **11** (1963) 72.
10. G. THOMAS and J. NUTTING, *J. Inst. Metals* **88** (1959/60) 81.
11. A. J. SEDRIKS, P. W. SLATTERY and E. N. PUGH, *Trans. ASM* **62** (1969) 815.
12. K. G. KENT, *J. Inst. Metals* **97** (1969) 127.
13. A. J. CORNISH and MISS M. K. B. DAY, *ibid* **99** (1971) 377.
14. M. ABE, K. ASANO and A. FUJIWARA, *Met. Trans.* **4** (1973) 1499.
15. B. I. EDELSON and W. M. BALDWIN JUN., *Trans. ASM* **55** (1962) 230.
16. C. D. BEACHEM, *ibid* **56** (1963) 318.
17. K. E. PUTTICK, *Phil. Mag.* **4** (1959) 964.
18. J. T. BARNBY, *Acta Met.* **15** (1967) 903.
19. H. W. HAYDEN and S. FLOREEN, *ibid* **17** (1969) 213.
20. J. GURLAND *ibid* **20** (1972) 735.
21. W. E. BROWER JUN., and S. N. SINGH, *Met. Trans.* **3** (1972) 3025.
22. S. GOTO and S. KODA, *J. Japan Inst. Light Metals* **24** (1974) 60 (in Japanese).
23. M. F. ASHBY, *Phil. Mag.* **14** (1966) 1157.
24. R. W. BAUER and H. G. F. WILSDOLF, *Scripta Met.* **7** (1973) 1213.
25. K. TANAKA, T. MORI and T. NAKAMURA, *Phil. Mag.* **21** (1970) 267.

Received 15 July and accepted 13 October 1975.